

# Unsupervised machine learning approaches to the $q$ -state Potts model

Andrea Tirelli,<sup>1</sup> Danyella O. Carvalho,<sup>2</sup> Lucas A. Oliveira,<sup>2,3</sup>  
J.P. Lima,<sup>2</sup> Natanael C. Costa,<sup>1,3</sup> and Raimundo R. dos Santos<sup>3</sup>

<sup>1</sup>*International School for Advanced Studies (SISSA), Via Bonomea 265, 34136 Trieste, Italy*

<sup>2</sup>*Departamento de Física, Universidade Federal do Piauí, 64049-550 Teresina PI, Brazil*

<sup>3</sup>*Instituto de Física, Universidade Federal do Rio de Janeiro Cx.P. 68.528, 21941-972 Rio de Janeiro RJ, Brazil*

(Dated: December 14, 2021)

In this paper we study phase transitions of the  $q$ -state Potts model, through a number of unsupervised machine learning techniques, namely Principal Component Analysis (PCA),  $k$ -means clustering, Uniform Manifold Approximation and Projection (UMAP), and Topological Data Analysis (TDA). Even though in all cases we are able to retrieve the correct critical temperatures  $T_c(q)$ , for  $q = 3, 4$  and  $5$ , results show that non-linear methods as UMAP and TDA are less dependent on finite size effects, while still being able to distinguish between first and second order phase transitions. This study may be considered as a benchmark for the use of different unsupervised machine learning algorithms in the investigation of phase transitions.

PACS numbers: 05.10.Ln, 05.70.Fh, 02.70.Uu

## I. INTRODUCTION

The study of phase transitions and critical phenomena is of crucial importance in Statistical Mechanics, [1, 2]. Numerical simulations, and most notably Monte Carlo methods, play a fundamental role in such a study. In most of cases, these numerical approaches are performed at finite-size systems, in which a careful analysis is required to avoid misleading results due to finite-size effects, in particular when dealing with phase transitions [3–6]. However, performing a finite-size scaling (FSS) analysis is a demanding task, being computationally costly to run simulations on large lattice sizes.

In view of this, it becomes increasingly important to devise techniques which can help in the identification of phase transitions, that are capable to give quantitatively accurate results for finite small system sizes. Over the past years, with the advent of powerful machine learning (ML) techniques, this goal has become more reachable, with these methods being applied in many different research areas. In the context of Condensed Matter and Statistical Physics, there has been a great effort to develop supervised and unsupervised ML techniques to identify different phases (from their particular patterns), as well as to examine phase transitions [7–9]. For instance, phase transitions have been examined by principal component analysis (PCA) [10–15], t-SNE [16–18], convolutional neural networks [19–24], restricted Boltzmann machines [25–27], intrinsic dimension analysis [28, 29], and persistence homology [30–36]. In particular, the use of persistence homology within Topological Data Analysis (TDA) seems a promising methodology to identify quantum critical points [36].

Despite the advances, the use of ML methods in these fields is still in its infancy, with their validation and usefulness to different problems being not entirely clear. We contribute to this discussion by performing a benchmark test for a number of unsupervised machine learning techniques, with the background of the classical  $q$ -state

Potts model [37]. This model describes interacting *classical spins* on a lattice, and has been used to capture the essential physics of a wide variety of systems, not necessarily magnetic [38]. It is a generalization of the Ising model, in the sense that the spin variable on each lattice site can take on  $q$  different values, instead of just two. Depending on the value of  $q$ , and of the dimensionality of the systems, the Potts model may exhibit first or second order phase transitions, with challenging finite-size effects. Therefore, we expect that the analysis of such a system may represent a testing ground to assess the performances and the weakness of a range of unsupervised ML algorithms.

In this work, we employ the following methods: (i) the Principal Component Analysis (PCA) [39], (ii) the  $k$ -means clustering [40], (iii) the Uniform Manifold Approximation and Projection (UMAP) [41], and (iv) the Topological Data Analysis (TDA) [42]. We use such algorithms to examine the phase transitions of the two-dimensional Potts model for  $q = 3, 4$ , and  $5$  – from snapshots generated by Monte Carlo simulations –, presenting their results for different system sizes. In what follows, the paper is organized as: the model is presented in the next Section, while the ML methodologies are outlined in Section III. Our results are presented and discussed in Section IV, with final remarks and conclusions being left to Section V.

## II. THE $q$ -STATE POTTS MODEL

The Potts model describes interacting *classical spins* on a lattice, with each spin having  $q$ -states [38]. It may also be thought of as a classical unit vector pointing along the vertices of a polygon with  $q$  sides, thus being oriented along a direction making an angle

$$\theta_n = \frac{2\pi n}{q}, \quad (1)$$

with some arbitrary direction, and where  $n = 0, 1, 2, \dots, q - 1$ . One may also formally treat  $q$  as a continuous parameter, and the limit  $q \rightarrow 1$  maps the model onto the percolation problem [38].

The Potts Hamiltonian reads

$$\mathcal{H} = -J \sum_{\langle i, j \rangle} \delta_{\theta_i, \theta_j}, \quad (2)$$

where the sum runs over a square lattice with periodic boundary conditions,  $\langle i, j \rangle$  denotes nearest neighbour sites, and  $J > 0$  is the ‘exchange’ coupling which sets the energy scale;  $\delta_{\theta_i, \theta_j}$  is the Kronecker delta function. The Hamiltonian is invariant under a discrete symmetry in which all spins are rotated by  $2\pi/q$ .

Most of the properties of the Potts model have been known for some time [38]. In particular, the critical temperature separating a ferromagnetic phase from a paramagnetic one on a square lattice is known from duality arguments to be [38]

$$T_c = \frac{J}{\ln(1 + \sqrt{q})}. \quad (3)$$

It should also be noted that in two dimensions the transition is continuous (or second order) if  $q \leq 4$ , and is discontinuous (first-order) if  $q > 4$  [38]; for the continuous transitions, the critical exponents are also known exactly [43]. In view of this wealth of exact data, the Potts model has been used to test many new methods, as in the current case of unsupervised machine learning techniques.

### III. METHODS

In this section we briefly describe the Machine Learning algorithms used in the analysis of phase transitions of the Potts model: all these techniques are *unsupervised* methods, i.e. methods working on unlabelled datasets, where the typical goals are to automatically find patterns within such data, or to reduce their dimensionality without loss of information. We resort to three methods. The first two, namely Principal Component Analysis and  $k$ -means clustering, though being quite standard and well-known in the machine learning community, have only recently been exploited to solve problems in Statistical Physics and Condensed Matter [10–12, 14, 16, 21]. The third method, Topological Data Analysis (TDA), represents a new class of techniques based on Applied Computational Topology [42], and it has been recently used in the study of phase transitions [31, 33, 34, 36].

In the present work, we follow the approach of Ref. [36], which has proven to be successful in the detection of quantum phase transitions, such as those described by the Hubbard model and the Periodic Anderson model. In addition, we will present some results obtained using the UMAP algorithm [41], which is a recent manifold learning technique for non-linear dimensionality reduction. In

a way, using UMAP corresponds to using PCA, but in non-linear, topology-oriented settings. In what follows, we present highlights of these three methods.

#### A. Principal Components Analysis

Principal Component Analysis (PCA) is a *linear* dimensionality-reduction technique whose primary scope is to reduce the dimensionality of data sets, by transforming the (often large) set of covariates into a smaller one, while still retaining most of the information in the original set of features. Of course, a reduction in the number of variables of a data set usually comes at the expense of accuracy, i.e. loss of information, but the trick in dimensionality reduction is to render information loss as small as possible, while obtaining a new dataset with a much smaller number of variables. Dimensionality reduction is often used as a preprocessing technique, where the reduced dataset created with PCA is then fed to a supervised machine learning model. In our case, the reduced data will be processed through a clustering method instead.

Let  $X$  denote a dataset, i.e. a matrix with  $n$  rows (samples) and  $m$  columns (features). We denote by  $X_i$  the  $i$ -th column of  $X$ . PCA [39, 44, 45] works through a number of computational steps as follows:

- *standardization*: each variable is properly scaled so that each contributes equally to the analysis. This corresponds to defining a new dataset  $X^{\text{std}}$ , such that,

$$X_i^{\text{std}} = \frac{X_i - \mu_i}{\sigma_i},$$

where  $\mu_i$  and  $\sigma_i$  are respectively the mean and the standard deviation of the vector  $X_i$ , and the operations of subtraction and division are performed component-wise;

- *covariance matrix computation*: this step is needed to investigate the presence of correlations between the features of  $X$ . The covariance matrix  $\text{Cov}(X)$  is defined as

$$\begin{aligned} \text{Cov}(X)_{i,j} &= \text{cov}(X_i, X_j) \\ &= \mathbb{E}((X_i - \mathbb{E}(X_i))(X_j - \mathbb{E}(X_j))), \end{aligned} \quad (4)$$

where  $\mathbb{E}$  stands for the mean value operation;

- *computation of the spectrum of  $\text{Cov}(X)$* : eigenvectors of the covariance matrix are the principal components and are derived from the initial features by performing linear combination. In a way, this can be interpreted as a *basis change* in the features space. The most important characteristics of these new features is that they are uncorrelated and most of the information within the initial variables is squeezed or compressed into the first components.

The main point is that usually most of the information of  $X$  is contained in the components whose corresponding eigenvalues have the highest modulus. As such, a new dataset  $\bar{X}$  can be constructed as follows: the  $i$ -th column  $\bar{X}_i$  of  $\bar{X}$  is the  $i$ -th eigenvector of  $\text{Cov}(X)$ , assuming that eigenvectors have been sorted in descending order, according to the magnitude of their eigenvalues. In most cases, such as those discussed here, one only selects the principal components whose eigenvalues are larger than a certain threshold: in this way we significantly reduce the dimensionality of the dataset, while retaining most of its information content. We note that, while being a very commonly used technique, PCA has some limitations: for example, it fails to detect *non-linear* correlations between features.

### B. $k$ -means clustering

$k$ -means is an algorithm that falls in the class of unsupervised machine learning methods [40, 46]: given a dataset  $X$  composed by  $n$  observations, its aim is to partition such samples into  $k$  clusters in which each observation belongs to the cluster with the nearest mean (cluster centres or cluster centroid), serving as a prototype of the cluster. The way in which  $k$ -means performs this task is by minimizing the within-cluster variances.

More formally, given a dataset  $X$ , i.e. a matrix  $X$  of dimension  $(n, m)$ , let  $x_i$  denote the  $i$ -th row, for  $i = 1, \dots, n$ .  $k$ -means aims to partition the samples  $x_1, \dots, x_n$  into  $k$  ( $k \leq n$ ) clusters  $C = \{C_1, \dots, C_k\}$  by optimizing the within-cluster sum of squares: therefore, the minimization problem can be written as

$$\operatorname{argmin}_C \sum_{i=1}^k \sum_{x \in C_i} \|x - \mu_i\|^2,$$

where  $\|\cdot\|$  denotes the Euclidean vector norm and  $\mu_i$  is the mean of points belonging to the cluster  $C_i$ ; such a mean is often called *centroid* of the cluster. Since solving exactly such a minimization problem is NP-hard [47], heuristic techniques are commonly used to obtain approximate solutions in polynomial time. On such technique is the following iterative algorithm:

- we start with an initial (random) assignment of the  $k$  centroids  $m_1^1, \dots, m_k^1$ ;
- we proceed by alternating an assignment step and an update step, until a certain stopping criterion is met.

In the assignment step, each observation is assigned to the cluster corresponding to the nearest centroid, with respect to the euclidean distance, so that the  $i$ -th cluster at iteration  $t$  can be written as

$$C_i^t = \{x : \|x - m_i^t\| \leq \|x - m_j^t\|, \forall j, 1 \leq j \leq k\}.$$

In the update step, the centroids are recomputed, with respect to the new partition into clusters generated by the assignment step,

$$m_i^{t+1} = \frac{1}{|S_i^t|} \sum_{x_j \in S_i^t} x_j$$

The algorithm has converged when the assignments no longer change. Although the algorithm is not guaranteed to find the optimum, [48], it normally produces a adequate partition of the dataset into clusters.

### C. Combining PCA and $k$ -means

Even though PCA and  $k$ -means perform two seemingly unrelated tasks, they are often combined during the unsupervised analysis of a dataset. In particular, given a dataset  $X$ , which might have a large number of samples and features, one first uses PCA to reduce the dimensionality, producing a new dataset  $\bar{X}$ , with less features, but retaining (most of) the information content of  $X$ . Cluster analysis is then performed on  $\bar{X}$  via  $k$ -means. Stacking together PCA and  $k$ -means in this way is a common practice, especially when the number of principal components is 2 or 3: in this case, samples on the initial dataset  $X$  can be visualized as points in the two-dimensional plane or three-dimensional space and clusters can be represented as coloured point clouds. This approach is the one adopted in the present work.

### D. UMAP

The mathematical foundations of the UMAP, which first appeared in [41], are advanced topics at the intersection between Riemannian Geometry and Algebraic Topology: as such, in contrast with PCA and  $k$ -means, explaining the details of such an algorithm is beyond the scope of this work and we just mention few of its main features. UMAP has proved to be a very efficient and scalable algorithm, with improved performances with respect to analogous non-linear dimensionality reduction techniques, such as  $t$ -SNE, [49]. Let  $X$  be a point-cloud and  $\tilde{X}$  be the non-linear projection of  $X$  to the feature space constructed by UMAP. The main point is that UMAP is capable to preserve as much as possible the global structure – topology – of  $X$  in the projection  $\tilde{X}$ . At its core, UMAP constructs a high dimensional graph representation of the data and then optimizes a corresponding low-dimensional graph representation to make it as structurally similar as possible to the higher dimensional one. The UMAP algorithm depends on several hyper-parameters: the most important one is  $n_{\text{neigh}}$ , the number of approximate nearest neighbours used to construct the initial high-dimensional graph. Indeed, such a parameter controls how UMAP balances local versus global structure – low values will push UMAP to focus

more on local structure by constraining the number of neighbouring points considered when analysing the data in high dimensions, while high values will push UMAP towards representing the big-picture structure while losing fine detail. In our case, we are interested in observing differences in the global structure of the data, for variations of the order parameter for the phase transition, so we shall use UMAP with a large value of  $n_{\text{neigh}}$ .

### E. Topological Data Analysis

Topological Data Analysis is a set of methods whose aim is to analyse datasets from the point of view of topology. If compared to PCA and  $k$ -means, TDA is the most mathematically involved theory and in this subsection we only mention the main points of the approach. In particular, we shall follow the pipeline devised in [36], which the reader is invited to consult for a detailed explanation of the various steps of the analysis.

The main aim of TDA is to use computational techniques coming from Applied Topology to describe a given dataset by a set of topological features, called persistence diagrams. Such features are computed via Persistence Homology [50], so that, if  $X$  is the dataset, interpreted as a point cloud in a higher-dimensional space, we obtain a set of topological features  $\mathcal{D}(X)$ . The set  $\mathcal{D}(X)$  depends on certain parameters, modelling the complexity of the topological invariants that one wishes to extract from  $X$ . Therefore, fixing such a set of topological invariants  $\mathcal{I}$ , one can build a map

$$X \longrightarrow \mathcal{D}_X, \quad (5)$$

by associating a point cloud  $X$  to its persistence diagram  $\mathcal{D}_X$ . With this mapping, also called *topological embedding* we can compare two different point clouds  $X_1$  and  $X_2$ : the way this comparison is performed is by endowing the space  $\mathcal{PD}$  of all persistence diagrams with a metric space structure, which can be done by exploiting the definitions of Wasserstein, Betti and Bottleneck distances between persistence diagrams. For more details, see, e.g., Ref. 36 and the references therein.

Being able to compare different point clouds in terms of their topological similarity, allows us to construct an algorithm that separates point clouds into clusters: given  $n$  point clouds,  $X_1, \dots, X_n$  (for the purposes of this work, one can assume  $X_i$  as a number of snapshots of spin configurations at a given temperature obtained through a Monte Carlo simulation), one can construct a square matrix  $M_X$  of dimension  $n$ ,  $M_X = (m_{ij})$ , by letting

$$m_{ij} = \tilde{d}(X_i, X_j), \quad (6)$$

where  $\tilde{d}$  is the distance measure constructed with persistence diagrams. The key point is that, the more the point clouds  $X_i$  and  $X_j$  are topologically similar, the smaller is the value  $\tilde{d}(X_i, X_j)$ . As such,  $M_X$  can be used, by means of *clustering algorithms*, to group together point clouds

that share the same topological features and separate those with an inherently different topology. Following [36], this is performed by using fuzzy spectral clustering, [51–53], for the identification of two clusters (one corresponding to point clouds below the critical temperature, the other for point cloud above the critical temperature). This leads to the construction of a membership degree function

$$l = (l_0, l_1) : \{X_1, \dots, X_n\} \rightarrow [0, 1]^2,$$

such that  $l_0(X_i)$  is the membership degree to the first cluster of the point cloud  $X_i$ ,  $l_1(X_i)$  is the membership degree to the second cluster of the point cloud  $X_i$ , and  $l_0(X_i) + l_1(X_i) = 1$  for all  $i$ . The key point is to analyse the sequence

$$\bar{l} = (l_0(X_1), \dots, l_0(X_n)). \quad (7)$$

This sequence can be segmented in smaller subsequences based on the range of variation of the membership degree; in particular, the critical point will be one of the endpoints (based on the position) of the longest quasi-constant subsequence of  $\bar{l}$ . Therefore, the critical point can be detected by a simple linear time algorithm that scans  $\bar{l}$  and identifies the longest quasi-constant subsequence.

## IV. RESULTS

We consider  $L \times L$  square lattices with periodic boundary conditions, whose spin configurations are sampled through standard Monte Carlo simulations with heat bath dynamics [54] according to the energetics specified by Eq. (2).

For the purposes of the Machine Learning methods discussed above, for fixed  $q$ , a spin configuration (or a snapshot) is stored in a vector,  $X_q$ , of length  $L^2$ . Through MC sampling, we generate  $m$  configurations at a given temperature, and we proceed analogously for a total of  $m \sim 20$  different temperatures, chosen in the neighbourhood (typically  $0.4T/J$ ) of the critical one. In so doing, the resulting dataset,  $X_q$ , is a matrix with dimension  $nm \times L^2$ , treating a single configuration as a row vector. In order to assess effects arising from the finite size of the lattices, we consider  $L = 20, 30, 40, 50, 60$ , and  $80$ . In what follows, we present our results and compare two approaches: the first combines PCA with  $k$ -means, while the second uses TDA, within the pipeline established in Ref. 36.

### A. Phase transitions via PCA + $k$ -means

The workflow combining PCA with  $k$ -means works as follows: viewing  $X_q$  as a feature matrix, using PCA we can select the principal components which retain most of the information of  $X_q$ , obtaining a new dataset  $\tilde{X}_q$  of

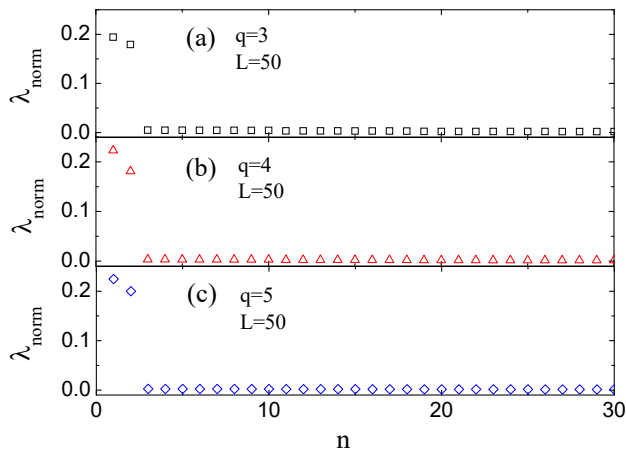


FIG. 1. PCA normalized eigenvalues for the Potts model for (a)  $q = 3$ , (b)  $q = 4$ , and (c)  $q = 5$ .

dimension  $nm \times k$ , with  $k \ll L^2$ , i.e. we embed the initial data points of  $X_q$  in the *PCA space*. We then run the  $k$ -means algorithm on  $\tilde{X}_q$ , to understand how the Monte Carlo snapshots are placed in the PCA space and if there is a relation between such a spatial distribution and the phase transition that the system undergoes. In Figure 1 we show, for  $q = 3, 4, 5$ , the values of the normalized eigenvalues of the first 30 principal components. We can see in all cases that the first two normalized eigenvalues are orders of magnitude larger than all the others. Therefore, when deciding the dimension of the PCA space which we embed the Monte Carlo snapshots, we can safely set  $k = 2$ , as the first two components already contain all the information of  $X_q$ . Let  $p_1$  and  $p_2$  denote the first two principal components. For a given snapshot  $x$ , we shall denote with  $p_i^x$ , for  $i = 1, 2$  the two-dimensional projection of  $x$ , given by the corresponding principal component; we then define the quantity

$$\gamma_x = \sqrt{\|p_1^x\|^2 + \|p_2^x\|^2},$$

which, if we average over all samples at a given temperature  $T$ , leads us to considering the quantity

$$\Gamma(T) = \mathbb{E}_{t(x)=T} \frac{\gamma_x}{L}, \quad (8)$$

where,  $t(x)$  denotes the temperature of the snapshot  $x$  and  $L$  is the lattice size. One can study the behaviour of  $\Gamma(T)$  as a function of the temperature, as shown in Figure 2. We can notice that,  $\Gamma$  is decreasing as a function of  $T$  and that the steepness of the descent increases around the transition temperature, while being of small magnitude away from it. Even though this behaviour is consistent for all values of  $L$ , we see that it is much more visible for larger lattice sizes, suggesting that there is a dependence from finite size effects. Another interesting quantity that one naturally considers in studying phase transitions is

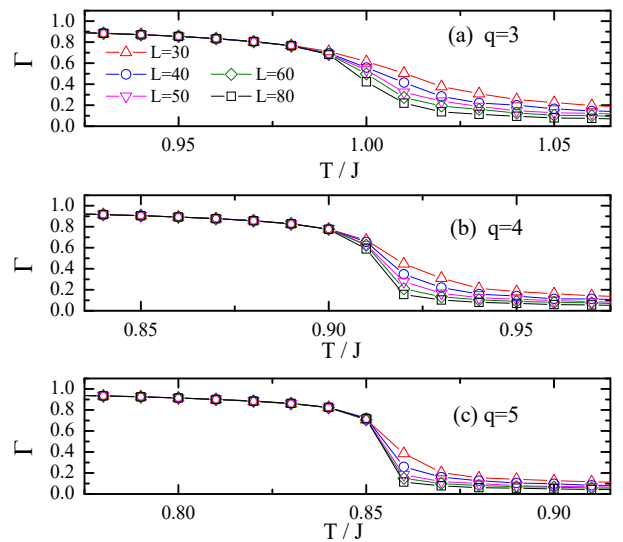


FIG. 2. The PCA order parameter,  $\Gamma$ , for (a)  $q = 3$ , (b)  $q = 4$ , and (c)  $q = 5$ .

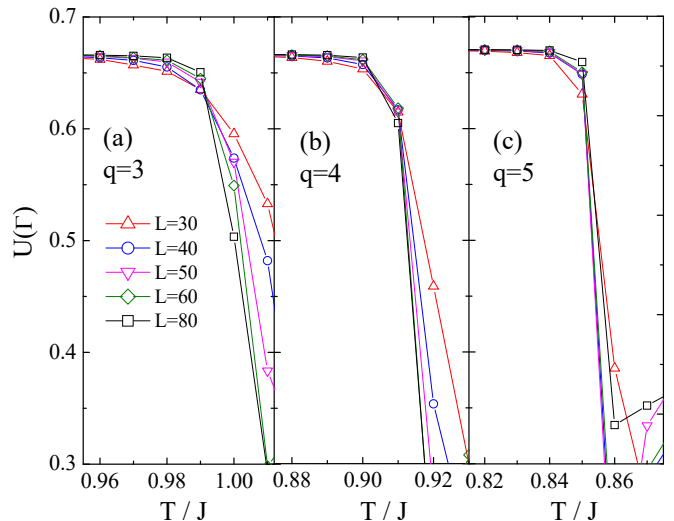


FIG. 3. The PCA ‘Binder cumulant’,  $U(\Gamma)$ , for (a)  $q = 3$ , (b)  $q = 4$ , and (c)  $q = 5$ .

the Binder cumulant, [55, 56] of  $\Gamma$ , which is the kurtosis of  $\Gamma$ , defined as

$$U(\Gamma) = 1 - \frac{\mathbb{E}_{t(x)=T} \frac{\gamma_x^4}{L}}{3 \mathbb{E}_{t(x)=T} \frac{\gamma_x^2}{L}}. \quad (9)$$

In Figure 3 we display, for different lattice sizes and all values of  $q$ ,  $U$  as a function of  $T$ . We see that, as expected, the behaviour of the Binder cumulant is very similar to that of  $\Gamma$ .

Finally, we conclude our analysis of the Potts model via PCA, by applying  $k$ -means on the principal components. In Figure 4 we show the corresponding results. For all

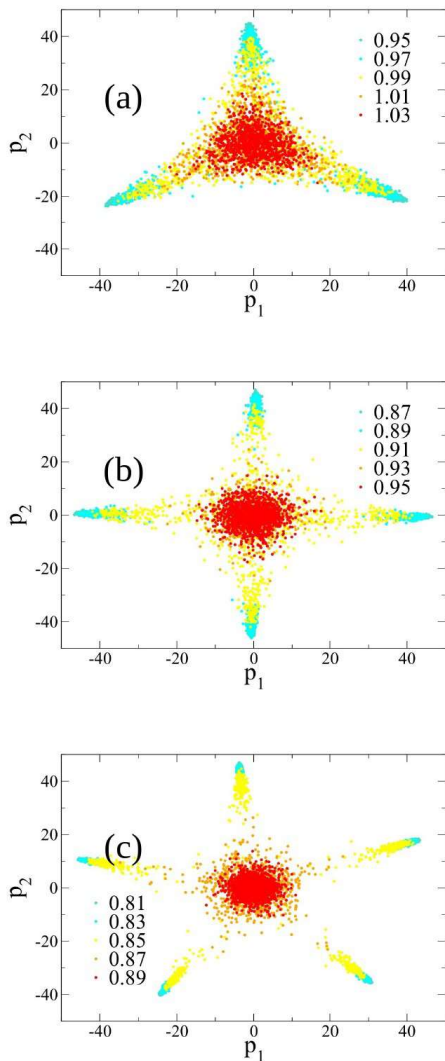


FIG. 4. Cluster division through the PCA algorithm around the critical point, for (a)  $q = 3$ , (b)  $q = 4$ , and (c)  $q = 5$ .

values of  $q$ , we see that samples at a temperature above the critical value  $T_c(q)$  tend to form a unique point cloud; on the other hand, snapshots at  $T$  below  $T_c(q)$  arrange themselves in clearly separated clusters, whose number is exactly  $q$ .

The division into separated clusters for temperatures higher than the critical value leads us to giving the following definition: given a  $k$ -means division into clusters,  $C_1, \dots, C_k$  let  $m_1, \dots, m_k$  the corresponding centroids. We consider the average distance of such centroids from the origin, i.e.  $\bar{m} = \frac{1}{k} \sum_{i=1}^k \|m_i\|$ . Note that this definition is well-given as the data have been normalized as a preprocessing step. In Figure 5 we plot  $\bar{m}$  against the temperature in the cases  $q = 3, 5$  both for  $N = 50$ . The behaviour of  $\bar{m}$  as a function of  $T$  is analogous to that of the  $\Gamma$  parameter, shown in Figure 2. Note that the steepness of the curve is significantly different in the two

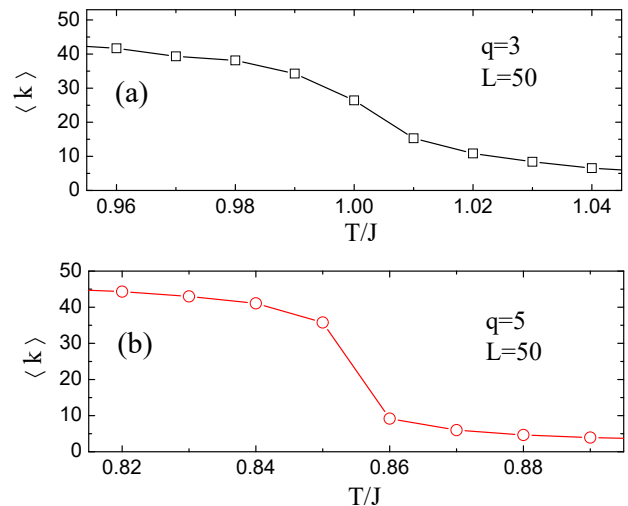


FIG. 5. Average distance from the origin of the  $k$ -centroids of the PCA point-clouds as a function of the temperature, fixing  $N = 50$ , for (a)  $q = 3$ , and (b)  $q = 5$ .

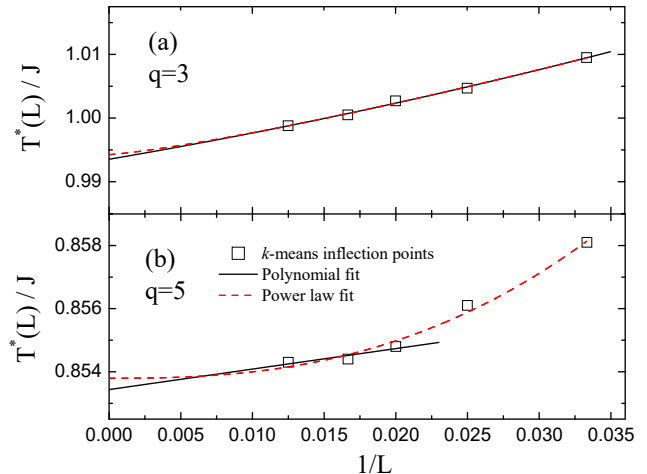


FIG. 6. Scaling analysis of the predicted transition points combining PCA and  $k$ -means, for (a)  $q = 3$ , and (b)  $q = 5$ . Solid black curves are polynomial fittings, while red dashed lines are power law ones.

cases: for  $q = 3$  we see a slow decrease to 0, in accordance to the fact that, in this case, the model exhibits a second order transition; on the other hand, for  $q = 5$ , where one sees a first order transition, the curve drops significantly to zero around the critical value  $T_c(5) = 0.851$ . Therefore, we can use  $\bar{m}$  to detect the critical point of the transition by identifying the point of steepest descent in the curve. Using this method to predict the critical point for a given lattice size, we performed a scaling analysis: Figure 6 show the corresponding results, by plotting the transition temperature as a function of the inverse of the lattice size. For  $q = 3$ , the interpolation at  $N \rightarrow \infty$  is well consistent with the reference values within our error bars.

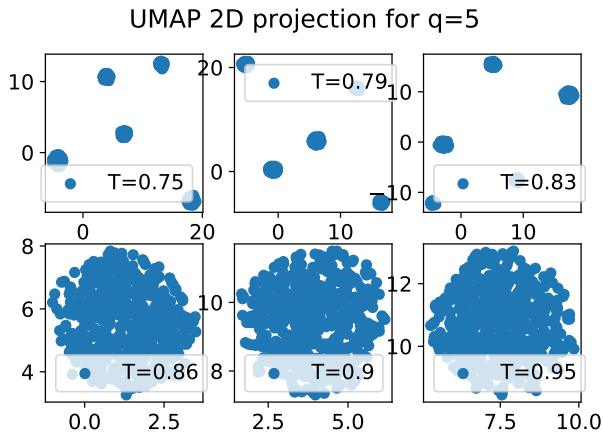


FIG. 7. UMAP projections onto a two-dimensional latent space, for  $q = 5$  and different values of the temperatures, around the critical one, whose value is 0.85.

### B. Phase transitions via UMAP

The analysis that we perform with the UMAP algorithm is very similar to the one using PCA reduction. Essentially, we project the dataset  $X_q$  onto a lower dimensional space and we investigate how variations of the order parameter around the transition point affect the arrangement of data points in the space. In Figure 7 we show one case of such dimensionality reduction, when  $q = 5$ . From (3), we know that in this case the critical temperature is given by  $T_c = 1/\ln(1 + \sqrt{5}) \approx 0.85$ : we see that data-points at temperatures below  $T_c$  arrange in order to form five well-separated clusters, whereas when  $T > T_c$  the corresponding Monte Carlo snapshots are all gathered in a single cluster. The projected points display a behaviour already observed in the previous subsection: for values below the critical temperature we observe the formation of clusters, whose quantity is the same as the number of ordered states of the system. On the other hand, for values above the critical temperature, the points tend to group around origin suggesting the non-existence of an ordered state. Even though this behaviour is in strong agreement with the one shown through PCA and  $k$ -means in the previous section, we notice that with UMAP the division in clusters for  $T < T_c$  is more uniform as well as the concentration in a single cloud for  $T > T_c$ . In a way, this shows the power of UMAP over PCA; indeed, UMAP is able to better capture the global structure of the data and, since the transition behaviour is strictly reflected by how spins place themselves over the lattice, this results in a much clearer distinction of the points arrangement in the projected space for different phases. This suggests that analysing the topological properties of data is fundamental for the detection phase transitions points.

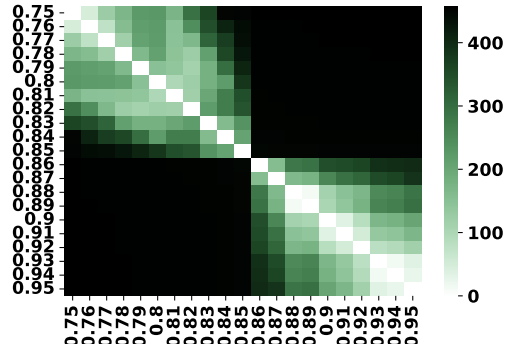


FIG. 8. Heat-map representing the distance matrix  $M$  for the  $q$ -state Potts model, for  $q = 5$  and  $N = 80$ , using the Betti distance, with  $p = 2$ ; column labels are the different values of the temperature  $T$ .

### C. Phase transitions via TDA

The importance of analysing the topology of data, showcased by the improvement of UMAP over PCA, is further enhanced by our results on the application of TDA to the Potts model. We proceed as in [36]: first, using TDA, we project data-points into the persistence space and then, with fuzzy spectral clustering, we assign a membership-score to each point-cloud at given temperature.

In Figure 8 we show a heat-map representation of the distance matrix constructed from persistence diagrams, in the case  $q = 5$  and  $N = 80$ : as expected, one can identify two darker clusters in the bottom-left and upper-right zones, and also two lighter clusters in the upper-left and bottom-right zones. This suggests that: (1) the point-clouds corresponding to temperatures  $T$  in the range from 0.75 to 0.85 are all topologically similar as well as point clouds in the range from 0.86 to 0.95; (2) a point cloud corresponding to a temperature  $T$  for  $0.75 \leq T \leq 0.85$  is topologically different from all point-clouds in the range  $[0.86, 0.95]$  and vice-versa.

The expectation is that data within the same phase should have similar scores. This expectation is fully met: in Figure 9 we plot, for  $q = 3, 4, 5$  and the corresponding ranges of lattice sizes, the fuzzy membership degree curves for datasets  $X_q$ . In all cases, the curve is almost constantly equal to 1 up to the critical temperature  $T_c(q)$ , after which the values drastically drop and remain close to 0. One important aspect to notice is that this behaviour is completely independent of the size of the lattice: indeed, for every value of  $q$ , all the curves, each of which is relative to specific value of the lattice size, are fully overlapping. This suggests that our the algorithmic pipeline for the identification of transition points is not affected by finite size effects, as opposed to PCA, as shown in Figures 2 and 3. In Figure 10 we show the relationship between transition points and lattice size, which makes explicit the independence of the method of the lat-

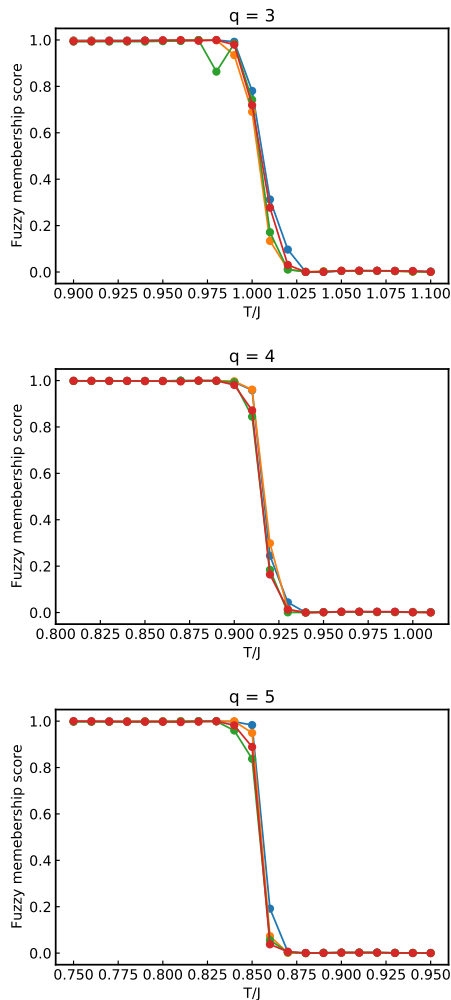


FIG. 9. Fuzzy membership degree vector for the analysed temperatures in the  $q$ -state Potts model as a function of the lattice size for  $q = 3$ ,  $q = 4$  and  $q = 5$ . In all cases the fuzzy membership function is able to perfectly discriminate between the two transitions, allowing a precise detection of the critical temperature.

ter quantity. Moreover, we see that, around their transition points, the slope of the membership lines for  $q = 3$  is smaller than when  $q = 5$ ; this leads us to conclude that, to some extent, TDA, through the membership functions, is able to capture some important physical aspects of the system: namely, the method can distinguish between a first order transition, i.e. when  $q = 5$ , and a second order transition, i.e. when  $q = 3$ .

## V. CONCLUSION

In this work we studied phase transitions of the  $q$ -state Potts model using a series of unsupervised Machine Learning algorithms: we employed classical techniques, such as PCA and  $k$ -means, and also benchmarked some

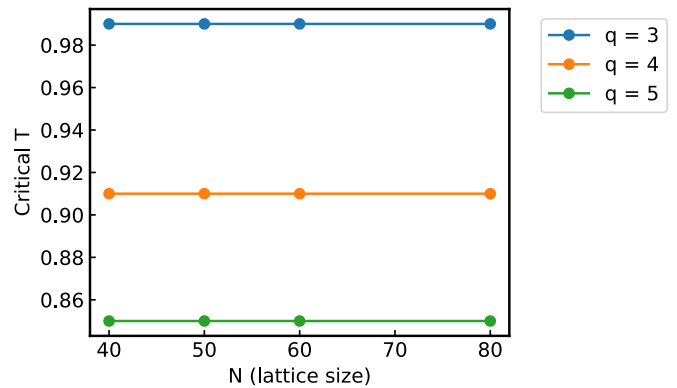


FIG. 10. Critical temperature of the  $q$ -state Potts model as a function of the lattice size for  $q = 3$ ,  $q = 4$  and  $q = 5$ . As it can be noticed, the TDA technique does not require finite size scaling, as the transition temperature are fully independent from the lattice size.

new methods coming from Algebraic Topology, such as UMAP and the TDA pipeline of [36]. We studied the Potts model for  $q = 3, 4, 5$  and in all cases we were able to correctly predict the critical temperature  $T_c(q)$  of the phase transition of the system.

As far as our main results are concerned, we found a very good agreement with the expected critical points provided by theoretical analysis of the model. All models have provided the exact results within error bars. Furthermore, we also found that linear techniques are more affected by finite size effects than non-linear ones; in particular, TDA has proved to be a powerful tool: on the one hand, the critical points using such a method are exact within the error bars for all the tested lattice sizes; on the other hand, using fuzzy membership scores, TDA can distinguish between first and second order transitions, which appear in the Potts model for  $q = 5$  and  $q = 3$ , respectively.

Therefore, we expect that this range of unsupervised machine learning methodologies could be a useful tool when studying hard problems for which standard techniques still give inconclusive answers, for both classical and quantum systems.

## ACKNOWLEDGMENTS

A.T. acknowledges financial support from the MIUR Progetti di Ricerca di Rilevante Interesse Nazionale (PRIN) Bando 2017 - grant 2017BZPKSZ. A.T. and N.C.C. acknowledge CINECA for awarding them access to the Marconi100 supercomputer, through the ISCRA framework, within the projects AI-H-QMC - HP10BGJH1X, and IsB23 (ISCRA-HP10BF65I0). D.O.C., L.A.O., J.P.L., N.C.C., and R.R.S. are grateful to the Brazilian Agencies National Council for Scientific and Technological Development (CNPq), National Coun-

cil for the Improvement of Higher Education (CAPES), FAPERJ, and FAPEPI for partially funding this project.

- 
- [1] H. E. Stanley, *Rev. Mod. Phys.* **71**, S358 (1999).
- [2] I. Herbut, *A modern approach to critical phenomena* (Cambridge University Press, Cambridge, England, 2007).
- [3] D. Landau and K. Binder, *A guide to Monte Carlo simulations in statistical physics* (Cambridge University Press, Cambridge, UK, 2021).
- [4] A. W. Sandvik, in *AIP Conference Proceedings*, Vol. 1297 (American Institute of Physics, 2010) pp. 135–338.
- [5] J. Gubernatis, N. Kawashima, and P. Werner, *Quantum Monte Carlo Methods: Algorithms for Lattice Models* (Cambridge University Press, Cambridge, England, 2016).
- [6] F. Becca and S. Sorella, *Quantum Monte Carlo approaches for correlated systems* (Cambridge University Press, Cambridge, England, 2017).
- [7] V. Dunjko and H. J. Briegel, *Reports on Progress in Physics* **81**, 074001 (2018).
- [8] G. Carleo, I. Cirac, K. Cranmer, L. Daudet, M. Schuld, N. Tishby, L. Vogt-Maranto, and L. Zdeborová, *Rev. Mod. Phys.* **91**, 045002 (2019).
- [9] J. Carrasquilla, *Advances in Physics: X* **5**, 1797528 (2020).
- [10] L. Wang, *Phys. Rev. B* **94**, 195105 (2016).
- [11] W. Hu, R. R. P. Singh, and R. T. Scalettar, *Phys. Rev. E* **95**, 062122 (2017).
- [12] N. C. Costa, W. Hu, Z. J. Bai, R. T. Scalettar, and R. R. P. Singh, *Phys. Rev. B* **96**, 195138 (2017).
- [13] C. Wang and H. Zhai, *Phys. Rev. B* **96**, 144432 (2017).
- [14] C. Wang and H. Zhai, *Frontiers of Physics* **13**, 1 (2018).
- [15] E. Khatami, *Journal of Physics: Conference Series* **1290**, 012006 (2019).
- [16] S. J. Wetzel, *Phys. Rev. E* **96**, 022140 (2017).
- [17] K. Ch’ng, N. Vazquez, and E. Khatami, *Phys. Rev. E* **97**, 013306 (2018).
- [18] W. Zhang, J. Liu, and T.-C. Wei, *Phys. Rev. E* **99**, 032142 (2019).
- [19] K. Ch’ng, J. Carrasquilla, R. G. Melko, and E. Khatami, *Phys. Rev. X* **7**, 031038 (2017).
- [20] P. Broecker, J. Carrasquilla, R. G. Melko, and S. Trebst, *Scientific reports* **7**, 1 (2017).
- [21] J. Carrasquilla and R. G. Melko, *Nature Physics* **13**, 431 (2017).
- [22] D. Kim and D.-H. Kim, *Phys. Rev. E* **98**, 022138 (2018).
- [23] P. Zhang, H. Shen, and H. Zhai, *Phys. Rev. Lett.* **120**, 066401 (2018).
- [24] E. Khatami, E. Guardado-Sanchez, B. M. Spar, J. F. Carrasquilla, W. S. Bakr, and R. T. Scalettar, *Phys. Rev. A* **102**, 033326 (2020).
- [25] Y. Nomura, A. S. Darmawan, Y. Yamaji, and M. Imada, *Phys. Rev. B* **96**, 205152 (2017).
- [26] L. Huang and L. Wang, *Phys. Rev. B* **95**, 035105 (2017).
- [27] R. G. Melko, G. Carleo, J. Carrasquilla, and J. I. Cirac, *Nature Physics* **15**, 887 (2019).
- [28] T. Mendes-Santos, X. Turkeshi, M. Dalmonte, and A. Rodriguez, *Phys. Rev. X* **11**, 011040 (2021).
- [29] T. Mendes-Santos, A. Angelone, A. Rodriguez, R. Fazio, and M. Dalmonte, *PRX Quantum* **2**, 030332 (2021).
- [30] I. Donato, M. Gori, M. Pettini, G. Petri, S. De Nigris, R. Franzosi, and F. Vaccarino, *Phys. Rev. E* **93**, 052138 (2016).
- [31] Q. H. Tran, M. Chen, and Y. Hasegawa, *Phys. Rev. E* **103**, 052127 (2021).
- [32] M. Feng and M. A. Porter, *Phys. Rev. Research* **2**, 033426 (2020).
- [33] B. Olsthoorn, J. Hellsvik, and A. V. Balatsky, *Phys. Rev. Research* **2**, 043308 (2020).
- [34] D. Leykam and D. G. Angelakis, *APL Photonics* **6**, 030802 (2021).
- [35] K. Kashiwa, T. Hirakida, and H. Kouno, arXiv:2103.12554 (2021).
- [36] A. Tirelli and N. C. Costa, arXiv preprint arXiv:2109.09555 (2021).
- [37] R. B. Potts, *Mathematical Proceedings of the Cambridge Philosophical Society* **48**, 106–109 (1952).
- [38] F.-Y. Wu, *Reviews of modern physics* **54**, 235 (1982).
- [39] S. Wold, K. Esbensen, and P. Geladi, *Chemometrics and intelligent laboratory systems* **2**, 37 (1987).
- [40] J. MacQueen *et al.*, in *Proceedings of the fifth Berkeley symposium on mathematical statistics and probability*, Vol. 1 (Oakland, CA, USA, 1967) pp. 281–297.
- [41] L. McInnes, J. Healy, and J. Melville, arXiv preprint arXiv:1802.03426 (2018).
- [42] G. Carlsson, *Bulletin of the American Mathematical Society* **46**, 255 (2009).
- [43] M. P. M. den Nijs, *Journal of Physics A: Mathematical and General* **12**, 1857 (1979).
- [44] H. Abdi and L. J. Williams, *Wiley interdisciplinary reviews: computational statistics* **2**, 433 (2010).
- [45] M. Ringnér, *Nature biotechnology* **26**, 303 (2008).
- [46] H. Steinhaus *et al.*, *Bull. Acad. Polon. Sci* **1**, 801 (1956).
- [47] M. Mahajan, P. Nimbhorkar, and K. Varadarajan, *Theoretical Computer Science* **442**, 13 (2012), special Issue on the Workshop on Algorithms and Computation (WALCOM 2009).
- [48] J. A. Hartigan and M. A. Wong, *Journal of the royal statistical society* **28**, 100 (1979).
- [49] L. Van der Maaten and G. Hinton, *Journal of machine learning research* **9** (2008).
- [50] H. Edelsbrunner and J. Harer, *Computational topology: an introduction* (American Mathematical Soc., 2010).
- [51] U. Von Luxburg, *Statistics and computing* **17**, 395 (2007).
- [52] J. Liu and J. Han, in *Data Clustering* (Chapman and Hall/CRC, 2018) pp. 177–200.
- [53] R. Jimenez, *Rock mechanics and rock engineering* **41**, 929 (2008).
- [54] F. Matsubara, A. Sato, O. Koseki, and T. Shirakura, *Physical review letters* **78**, 3237 (1997).
- [55] K. Binder, *Zeitschrift für Physik B Condensed Matter* **43**, 119 (1981).
- [56] K. Binder, *Physical Review Letters* **47**, 693 (1981).